Hindered Settling of Rod-Like Particles Measured with Magnetic Resonance Imaging

Michael A. Turney, Man Ken Cheung, and Robert L. Powell
Dept. of Chemical Engineering, University of California, Davis, CA 95616

Michael J. McCarthy
Dept. of Biological and Agricultural Engineering, University of California, Davis, CA 95616

Magnetic resonance imaging (MRI) is used to measure the time evolution of the volume fraction vs. height profile during batch sedimentation of rod-like particle suspensions. At any instant during sedimentation, MRI clearly delineates the supernatant, suspension, and sediment regions. The rod-like particles with a mean aspect ratio of 17.4 exhibit considerably larger hindered settling effects than spherical particles with increasing particle concentrations. This can be attributed in part to the larger increase in interparticle forces and relative viscosities with suspensions of rod-like particles than with suspensions of spherical particles, as the particle concentration increases. The relative viscosity of the rod-like particle suspensions is a function of the spin-spin relaxation time, T_2. Since T_2 is a measurable MRI quantity, this suggests that MRI may be used as an instrument for rheological measurement.

Introduction

Sedimentation is an important industrial means of concentrating suspensions of particles. There is extensive literature related to the sedimentation of spherical particles (Davis and Acrivos, 1985); however, very little work has been conducted concerning sedimentation of nonspherical particles. Despite its importance in the processing of fibrous materials such as tomato paste and paper pulp, sedimentation of fibers is neither well understood nor extensively studied. The relationship between particle shape and suspension dynamics is an important aspect in the design of the processing equipment as well as product development. It is also important in clinical applications, because the shape of red blood cells plays a role in their sedimentation rates (Reinhart et al., 1989).

Magnetic resonance imaging (MRI) exploits the interaction between radio-frequency and nuclei, most commonly ^1H, to reveal compositional and structural information. The spatial location of the excited nuclei within a material can be encoded by applying several magnetic field gradients (Morris, 1986). MRI can quickly and noninvasively measure the particle volume fraction as a function of time and position within a sedimenting suspension (Lee et al., 1992). X-ray tomography was used successfully in monitoring batch sedimentation of stable and flocculated spherical particles as a function of time and position (Auzerais et al., 1990). Although X-ray tomography can be a complementary imaging method to MRI, it is restricted to slow settling suspensions.

This work studies the relationship between particle geometry and sedimentation by measuring the time evolution of the volume fraction vs. height profiles of rod-like particle suspensions with MRI. Earlier studies of spherical particle behavior is used as a basis to understand rod-like particle suspensions.

Materials and Methods

Materials

The rod-like particles consisting of chopped rayon fibers (AB Bernhard Steffert, Sweden) were washed in soap and water, and were air dried prior to use. The criterion of Forgacs and Mason (1959) indicates that the onset of bending of these fibers occurs at shear rates of about 500 s^{-1} (Milliken et al., 1989). This shear rate is greater than the estimated shear rate obtained by assuming sedimentation of a single rod at low Reynolds number, $U_o/2a = 3.3\ s^{-1}$, where U_o is the Stokes velocity and a is the mean particle radius. Therefore, these fibers are assumed rigid.

Correspondence concerning this article should be addressed to M. J. McCarthy.

Table 1. Physical Properties of Particles and Suspending Fluid

Property	Units	Value
Particles: Rayon Fibers		
Density, ρ	kg/m^3	1,950
Dia., d	μm	19.3 ± 3.3
Length, L	μm	323.3 ± 23.4
Aspect Ratio, a_r	-	17.4 ± 4.3
Equiv. Dia., d_e	μm	57.1
Sphericity*	-	0.507
Vol., V	m^3	$9.7(\pm 3.2) \times 10^{-14}$
Suspending Fluid: UCON 50-HB-55		
Density, ρ_m	kg/m^3	970
Viscosity, μ	mPa·s	16.7

*Surface sphericity is defined as $\left(\frac{\text{surface area of a sphere}}{\text{surface area of a fiber}}\right)_{\text{equal volume}}$ (Becker, 1959).

The dimensions of these particles were obtained from scanning electron micrographs. These fibers are considered to be needle shaped, due to the presence of their irregular ends. The particle density was found by first weighing the particles in a volumetric flask with a Fisher Scientific Model XA analytical balance. A known quantity of water was then added to the flask which was weighed again.

The suspending fluid was UCON 50-HB-55 polyalkylene glycol (Union Carbide Corp., Danbury, CT). This fluid allowed sedimentation rates to be sufficiently slow for adequate time resolution in the MRI measurement. Additionally, the fluid yields good MRI signals with respect to the hydrogen nuclei. The viscosity was measured at 21.5°C with a Cannon-Ubbelohde dilution type viscometer. Physical properties of the particles and the suspending fluid are listed in Table 1.

Methods

All experiments were carried out using a 2-Tesla Oxford Instruments magnet with a General Electric CSI spectrometer. Cubic sedimentation vessels having interior dimensions of 4.5 cm were constructed from Plexiglas. A standard multiple spin-echo imaging sequence was used to image the sedimentation profiles (Morris, 1986). The parameters used in this sequence are listed in Table 2.

Wall effects are related to the rod dimensions relative to the width of the vessel (Morrison, 1989). Such effects are neglected in the present study, because the ratios L/W (L being the length of fiber, and W being the width of sedimentation vessel) and d/W (d being the mean particle diameter) are 7.2×10^{-3} and 4.3×10^{-4}, respectively.

We began our experiments with a low concentration suspension first, and then subsequent higher concentrations were obtained by adding known quantities of the rayon fibers. Mixing of the suspensions was accomplished by stirring continuously until the suspensions were homogeneously dispersed. The effectiveness of this mixing was checked by the initial MRI volume fraction measurements across the height of the vessel. There were no visible air bubbles in the suspensions when mixing was complete.

MRI measurements of the suspending fluid sample were made prior to each sedimentation experiment. This blank sample was placed at the same location inside the magnet as the sedimenting suspension. Because signal intensities are proportional to mobile hydrogen nuclei density and are negligible for the rayon fibers, volume fractions, ϕ, can be determined by the relation:

Table 2. Multiple Spin-Echo Pulse Sequence Parameters

Parameter	Value	Units
Predelay Time	100	ms
Echo Time	15, 50, 100	ms
Slice Thickness	10	mm
In-Plane Resolution	256	points
Field of View	60.33	mm
Readout Gradient Strength	425	Hz/mm
Number of Acquisition	2	-
Slice-selection Method: One-lobe sinc pulse with a trapezoidal gradient shape.		

$$\phi(h,t) = 1 - \frac{S_{os}(h,t)}{S_{ob}(h)} \tag{1}$$

where S_{ob} and S_{os} are the signal intensities along the vertical axis of the vessel for the blank and sedimenting suspension samples, respectively. Equation 1 allows for a complete description of volume fraction, ϕ, as a function of height measured from the top of the supernatant liquid, h, and time, t. Normally, the detected signal intensities are not equal to S_{os} and S_{ob}, because the detected signals are subjected to spin-lattice (T_1) and spin-spin (T_2) relaxation effects and so these relaxation effects must be corrected to obtain S_{os} and S_{ob} before Eq. 1 can be used.

The spin-lattice relaxation time, T_1, is found to be independent of particle volume fraction even up to the maximum packing fraction of the sediment. Spatially resolved T_1 measurements were obtained on a settled suspension using the FAst, VOlume-Resolved Immediate T_1 Estimation (FAVORITE) pulse sequence, which has been used to measure T_1 values of creaming oil-water emulsion by Kauten et al. (1991). This pulse sequence is a spatially selective version of a nonselective sequence introduced by Canet and co-workers (Canet et al., 1988; Fanni et al., 1989). The selective spin echo segments were separated from 180° inversion pulses by delays (τ), which allowed magnetization from the selected planar volume to undergo T_1 relaxation. The degree of spin-lattice relaxation after τ (300 ms) is measured by the ratio of signal 2 to signal 1 (S_2/S_1). The ratio of signal intensities provides a measure of the spin-lattice relaxation time:

$$T_1 = \frac{-\tau}{\ln\left(1 - \frac{S_2(h)}{S_1(h)}\right)} \tag{2}$$

A vertical plane was selected such that S_1 and S_2 become functions of the sample height. The projection data were obtained by repeating the pulse sequence experiment four times (four acquisitions) and adding the results together.

To check the measurements obtained using the FAVORITE sequence, T_1 measurements were also conducted using the standard inversion recovery technique. This method yields a

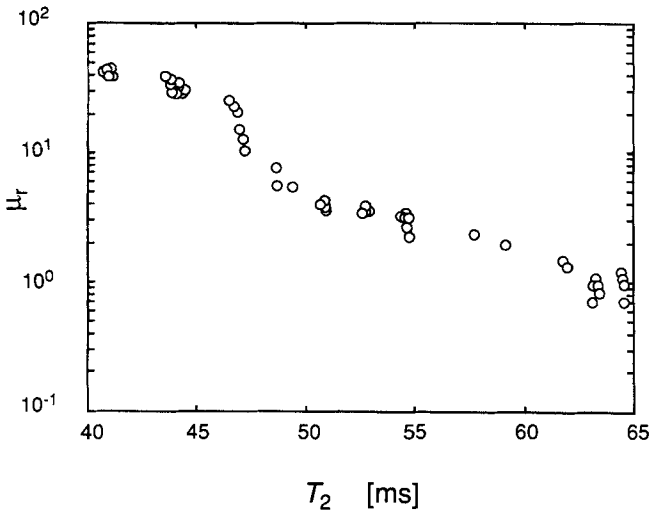

Figure 1. Dependence of relative viscosity on T_2.
Relative viscosity data were obtained from Milliken et al. (1989).

T_1 of 344 ms for the suspending fluid only. This value agrees with the measurements by the FAVORITE method.

Since τ is smaller than $5T_1$, the spin system has not been completely restored to equilibrium, and the signal intensity at a given settling time t is weighted according to:

$$S_s(h,t) = S_{\infty s}(h,t)\left[1 - \exp\left(\frac{-\tau}{T_1}\right)\right] \tag{3}$$

Similarly, with the same delay, for the suspending fluid only:

$$S_b(h) = S_{\infty b}(h)\left[1 - \exp\left(\frac{-\tau}{T_1}\right)\right] \tag{4}$$

Knowledge of the absolute signal intensity values are not important for the present study. However, it is extremely important to determine the relative signal intensities of the suspension with respect to the blank. Both experiments were conducted using equal delays then:

$$\frac{S_{\infty s}(h,t)}{S_{\infty b}(h)} = \frac{S_s(h,t)}{S_b(h)} \tag{5}$$

As a result, T_1 weighting of the signal intensities does not affect the measurement of volume fractions.

The spin-spin relaxation time, T_2, on the other hand is a strong function of volume fraction. The signal intensities obtained from a suspension become weighted by these spin-spin relaxation effects because of the functional dependence on $T_2(\phi)$, while those obtained from the suspending fluid only are not. This indicates that signals obtained from a fluid in a suspension will not be comparable to that of the blank. Therefore, corrections of the signals based upon these spin-spin relaxation effects were made.

Spatially resolved T_2 values and sedimentation profiles were measured with the Hahn multiple spin-echo sequence (Morris, 1986). To minimize motional effects in the MRI image, two acquisitions were obtained with a 1.5 s predelay. Signal intensities S_s' were obtained across the height of the sample at echo times (t_e)15, 50, and 100 ms. The plots of ln (S_s') vs. t_e were linear, and so S_s' is T_2 weighted according to:

$$S_s'(h,t) = S_{os}(h,t)\exp\left(\frac{-t_e}{T_2(h,t)}\right) \tag{6}$$

The least-squares fits of ln (S_s') vs. t_e allow for T_2 to be measured as a function of vertical sample position. $T_2(h,t)$ values ranging from 64 ms to 41 ms were measured for the supernatant liquid and the loosely packed sediment, respectively.

The T_2 corrected signals $S_{os}(h,t)$ were determined by extrapolation to $t_e = 0$ according to Eq. 6. In a similar fashion, T_2 corrected signals $S_{ob}(h)$ for the blank were determined.

The corrected signals of the suspending fluid, $S_{ob}(h)$, and partially sedimented suspension sample, $S_{os}(h,t)$, are then used to calculate the volume fraction according to Eq. 1.

Results and Discussion

Significance of $T_2(\phi)$

$\phi(h,t)$ can be combined with $T_2(h,t)$ to obtain $T_2(\phi)$. We found that a second-order polynomial adequately fit our data:

$$T_2(\phi) = 181.9\phi^2 - 126.9\phi + 63.32 \tag{7}$$

Knowledge of $T_2(\phi)$ for the rayon fibers suspended in UCON 50-HB-55 given by Eq. 7 is of physical importance, and is helpful as a cross-check on the use of Eqs. 1 and 6 because T_2 can be determined independently of S_s'. It is well-known that the viscosity of a suspension is a function of its volume fraction (Milliken et al., 1989). For suspensions of $a_r = 19.8$ fibers this relation is described by:

$$\mu_r = 1 + 28.5\ \phi^{1.01}, \quad \phi < 0.125 \tag{8a}$$

$$\mu_r = 1 + 2{,}040\ \phi^{3.01}, \quad \phi > 0.125 \tag{8b}$$

If Eq. 8 also describes the present rayon fiber/UCON 50-HB-55 systems, then the relative viscosity, μ_r, can be expressed as a function of T_2 by combining Eqs. 7 and 8. The resulting function, $\mu_r(T_2)$, is illustrated in Figure 1.

It should be noted that the spin-spin relaxation time is also a function of the chemical and physical nature of the fluid/particle system. Therefore, the data shown in Figure 1 is not a universal curve, but a demonstration of the possibility of relating a rheological property to a measurable MRI parameter. We believe that this result represents a step towards the use of MRI as an instrument for rheological measurement.

Sedimentation profiles

Sedimentation experiments for ten different initial suspension volume fractions ranging from 0.035 to 0.118 were conducted. Typical sedimentation profiles from these experiments are shown in Figures 2 and 3 where the initial suspension volume fractions, ϕ_i, were 0.041 and 0.101, respectively. The vertical position along the height of the vessel has been normalized with respect to the distance from the vessel bottom to the supernatant/air interface. The profiles were obtained at 30.19-s intervals; however, the profiles shown in Figure 2 are

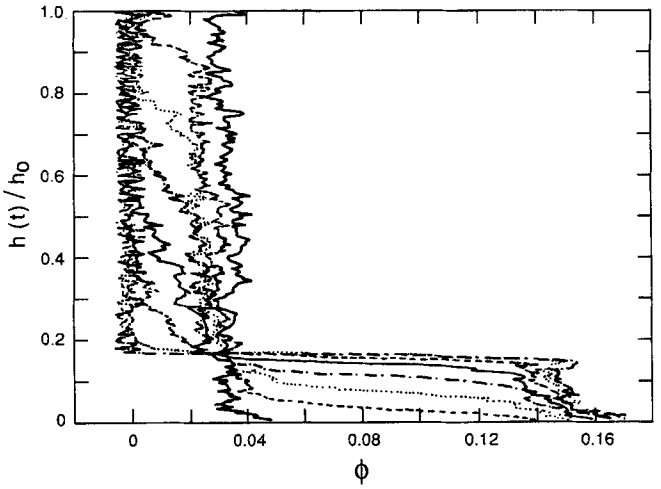

Figure 2. Volume fraction vs. normalized height profiles for a $\phi_l = 0.041$ suspension of $a_r = 17.4$ particles.

The profiles are shown at 120.76-s intervals to illustrate the time evolution of the supernatant, suspension, and loosely packed sediment regions.

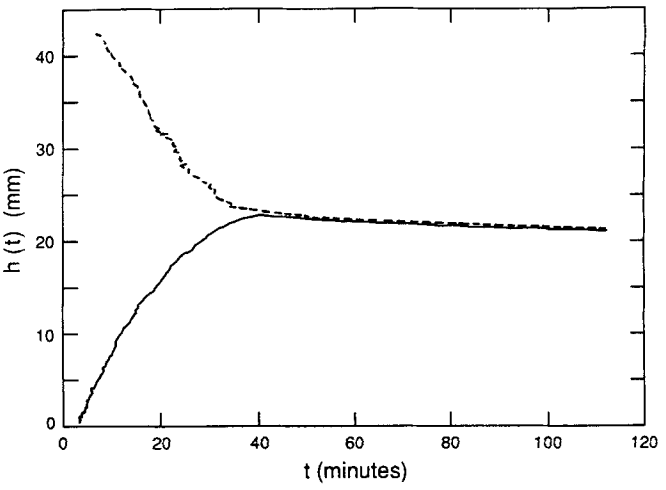

Figure 4. $\phi_l/2 = 0.05$ isoconcentration plane as a function of time for the data in Figure 3.

Dashed line shows the time evolution of the supernatant/suspension interface, whereas the isoconcentration plane of 0.128 (solid line) shows the rise of the sediment region.

separated by 120.76 s for clarity. The initial profile obtained illustrates a constant volume fraction across the height of the vessel; hence, the suspension was evenly mixed.

The resolution of the volume fraction profile measurements is limited by the 0.24-mm in-plane resolution and 10-mm slice thickness. This yields an approximately 0.58-mm^3 spatial resolution called a voxel. A more exact analysis of the structure of this voxel was determined by Maneval et al. (1990). Regardless of the exact voxel shape, this volume is considerably larger than the 9.7×10^{-5} mm^3 occupied by a single rayon fiber. Therefore, the presence of a few sparsely suspended particles in the supernatant region is not measured. The signal fluctuations shown in the supernatant region are assumed to be due solely to noise. The fluctuations in the solids volume fraction measurements in the supernatant region had a standard deviation of 0.003. Similarly, measurements of the suspension region had a standard deviation of 0.005. This indicates that the variation in measured signals in the suspension region are of the same scale as the supernatant region. Therefore, the small volume fraction fluctuations measured in the suspension region are attributed primarily to noise rather than to possible "clumping" of particles, and consequently the suspension is considered to be homogeneously dispersed.

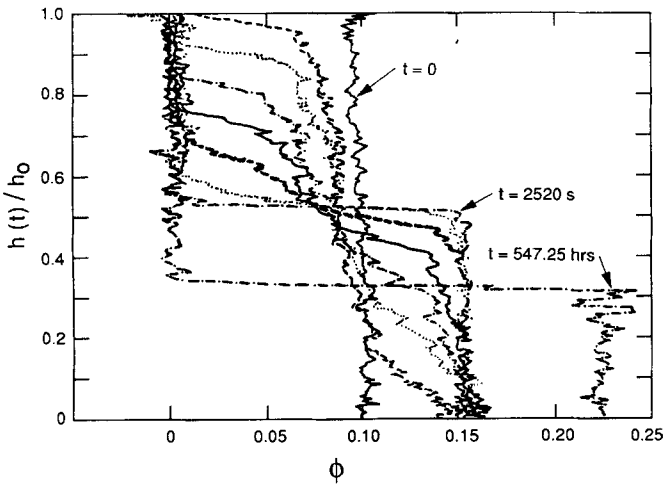

Figure 3. Volume fraction vs. normalized height profiles for a $\phi_l = 0.101$ suspension of $a_r = 17.4$ particles.

The profiles that are shown at 360-s intervals illustrate the early stages of sedimentation and the formation of the fan region as a loosely packed 0.155 vol. fraction sediment. On a longer time scale, the sediment packs to a vol. fraction of 0.225.

Spherical and rod-like particle systems both exhibit spreading of the supernatant/suspension interface, a suspension region of uniform volume fraction, as well as fan and sediment regions (Davis and Hassen, 1988; Lee et al., 1992). However, beyond these basic similarities, significant differences exist between the spherical and rod-like particle systems. For example, when the supernatant/suspension interface and fan have completely disappeared, the sediment of spherical particles attains a volume fraction of about 0.565, which indicates that the sediment has a disordered, close-packed structure (Russel et al., 1990). The sediment of our rod-like particles initially attains a volume fraction of 0.155, which suggests that the sediment structure is isotropic (Flory and Ronca, 1979). Then, the loosely packed sediment of the rod-like particles slowly becomes more tightly packed over time (Figure 3). Figure 4 indicates that this transition takes place at a decelerating rate. No further consolidation of the sediment takes place once a volume fraction of 0.225 is attained.

Hindered settling of rod-like particle suspensions

Extensive experimental and theoretical effort has been made to determine the hindered settling function, $f(\phi)$, for spherical particles (Barnea and Mizrahi, 1973; Buscall et al., 1982; Davis and Acrivos, 1985; Garside and Al-Dibouni, 1977; Richardson and Zaki, 1954). The function is defined so that the statistical

average particle settling velocity relative to the bulk suspension velocity is given by:

$$U = U_o f(\phi). \tag{9}$$

Here U_o is the terminal settling velocity of an isolated particle and ϕ is the local volume fraction of particles in the suspension. A common method of experimentally determining $f(\phi)$ is by measuring the fall velocity of the supernatant/suspension interface as the suspension settles. This velocity is measured for several different suspension concentrations, and $f(\phi)$ is reported as a function of ϕ_i, the initial suspension volume fraction.

Two significant difficulties arise in using this method to measure the hindered settling function. First, for dilute suspensions the position of the interface is difficult to define since it becomes increasingly diffuse as sedimentation proceeds. For spherical particles, interfacial spreading is due to particle polydispersity and self-induced hydrodynamic diffusion (Davis and Hassen, 1988). However, the position of the diffuse interface can be defined by the $\phi_i/2$ isoconcentration plane. The velocity of this isoconcentration plane has been found to be within 2% of the monodisperse suspension sedimentation velocity for spherical particles (Davis, 1988). Since the velocities are uniform throughout this central interface region, they can be accurately determined. For suspensions of rod-like particles, a similar technique is applied. The fall velocities for each of the suspension volume fractions are shown in Table 3.

The second difficulty arises from specifying the velocity of an isolated particle, U_o. A spherical particle settling through a Newtonian fluid in a large container at a small Reynolds number will attain a terminal velocity given by Stokes' Law. However, for rod-like particles the terminal settling velocity of a single rod-like particle in an unbounded fluid depends upon its orientation with respect to the direction of gravity. A rod-like particle settling with a small Reynolds Number ($Re < 0.1$) falls stably in its initial orientation (Happel and Brenner, 1983; Becker, 1959), that is, it neither rotates nor aligns with the gravity axis. The terminal velocity of a rod-like particle is described by U_1, U_2, and U_3, which are the 1st, 2nd, and 3rd component of the terminal velocity, respectively, where gravity acts in the direction parallel to U_3 (Happel and Brenner, 1983):

$$U_1 = \left[\frac{3}{2} - \ln(2a_r)\right]\frac{ga^2(\rho-\rho_m)}{8\mu}\sin 2\alpha \tag{10a}$$

$$U_2 = 0 \tag{10b}$$

$$U_3 = \left[\frac{3}{2} - \ln(2a_r)\right]\frac{ga^2(\rho-\rho_m)}{8\mu}\left[\frac{0.5 - 3\ln(2a_r)}{1.5 - \ln(2a_r)} + \cos(2\alpha)\right]. \tag{10c}$$

Here a is the mean rod radius, g is the gravitational constant, ρ and ρ_m are the densities of the particle and suspending medium, respectively. μ is the suspending fluid viscosity, and α represents the rod orientation angle with respect to the gravity axis. Equation 10a indicates that the particle will not fall completely in the direction of gravity. The extent of the lateral motion is a function of the particle geometry and fluid. The vertical velocity component, U_3 varies up to 50% with α. The suspensions being considered are initially randomly oriented. Hence, the U_o that is used to determine the hindered settling function is that resulting from repeated sedimentation experiments in which all particle orientations are realized. The resulting average is (Happel and Brenner, 1983):

$$U_o = \frac{gV(\rho-\rho_m)}{3\mu}\left(\frac{1}{K_1}+\frac{1}{K_2}+\frac{1}{K_3}\right). \tag{11}$$

Here V is the particle volume and K_1, K_2, and K_3 represent the components of the principal translational resistances of the particle. For a needle-shaped object these are:

$$K_1 = K_2 = \left(\frac{8\pi a_r}{\ln(2a_r) - 0.5}\right)a$$
$$K_3 = \left(\frac{4\pi a_r}{\ln(2a_r) - 0.5}\right)a. \tag{12}$$

The terminal settling velocity of a single needle-shaped particle averaged over all orientations, U_o, is determined from Eqs. 11 and 12.

Since the fiber aspect ratios are not uniform, we use the mean velocity $\langle U_o(a_r)\rangle$ to calculate the hindered settling function. The mean velocitiy $\langle U_o(a_r)\rangle$ based on the fibers shown on scanning electron micrographs is 5.44×10^{-5} m/s. It is important to note that $\langle U_o(a_r)\rangle$ is not equal to $U_o(\langle a_r\rangle)$, and that $\langle U_o(a_r)\rangle$ is the relevant quantity for determining the hindered settling function. Table 3 summarizes the measured fall velocities and the corresponding hindered settling functions.

To provide a basis for understanding the effect of particle geometry on the hindered settling function, in Figure 5, a comparison of the hindered settling function for the $a_r = 17.4$ rods to two common correlations for noncolloidal spheres is made (Barnea and Mizrahi, 1973; Richardson and Zaki, 1954). These are given by:

$$\frac{U(\phi)}{U_o} = \frac{(1-\phi)^2}{(1+\phi^{1/3})\exp\left(\frac{5\phi}{3(1-\phi)}\right)} \tag{13}$$

Table 3. Fall Velocity of Supernatant/Suspension Interface and Hindered Settling Function of $a_r = 17.4$ Rods

Vol. Fraction	Vel. of $\phi_i/2$ Isoconc. Plane (m/s)	U/U_o
0.035	4.20×10^{-5}	0.771
0.044	4.25×10^{-5}	0.779
0.045	3.92×10^{-5}	0.718
0.056	3.35×10^{-5}	0.614
0.058	3.12×10^{-5}	0.571
0.079	2.48×10^{-5}	0.457
0.091	1.95×10^{-5}	0.358
0.092	1.97×10^{-5}	0.360
0.105	1.63×10^{-5}	0.301
0.118	1.32×10^{-5}	0.242

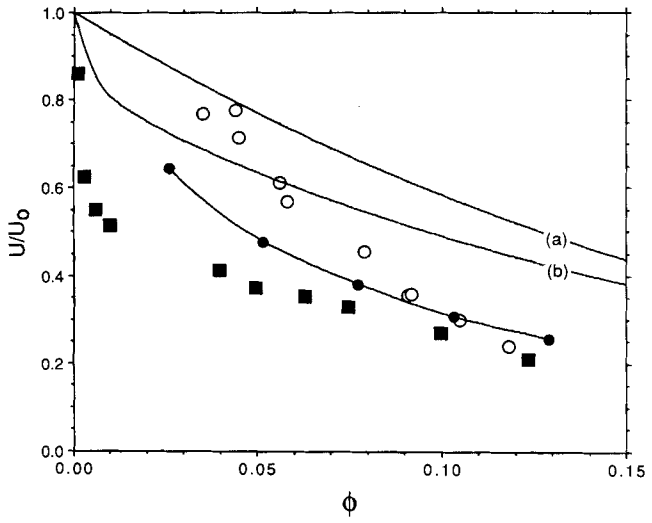

Figure 5. Measured hindered settling functions of $a_r = 17.4$ rod-like particles are shown as open circles.

The data of Anselmet (1989) for $a_r = 10$ particles are shown as solid squares. Rod-like particles settle much slower, especially at high volume fractions, than spherical particles as represented by (a) the Richardson and Zaki (1954) correlation with $n = 5.1$, and (b) the Barnea and Mizrahi (1973) correlation. Preliminary simulation results by Mackaplow and Shaqfeh (1993) for $a_r = 15.6$ particles are shown as solid circles.

$$\frac{U(\phi)}{U_o} = (1-\phi)^n \tag{14}$$

for the correlations of Barnea and Mizrahi (1973), and Richardson and Zaki (1954), respectively. Garside and Al-Dibouni (1977) find that an exponent of $n = 5.1$ gives the best correlation for spherical particles at creeping flow region.

As the volume fraction is increased, the hindered settling functions of spherical and rod-like particles differ significantly (Figure 5). The hindered settling function of rod-like particles is more strongly dependent on volume fraction than that for spherical particles. This phenomenon may be attributable to several factors. As the volume fraction is increased, interparticle forces between the rods become more significant than in the case of spheres, and tend to reduce the sedimentation rate. In addition, the slower settling rates of the rod-like particles could be attributed to differences in the relative viscosities between the two systems. A suspension of rod-like particles has a larger relative viscosity than a suspension of spheres of equal volume fraction (Milliken et al., 1989; Powell, 1991). As volume fraction increases, the difference in the relative viscosities between suspensions of rods and spheres also increases; consequently, the differences in settling rates also increases.

Beyond the present work, the most complete experimental study of sedimentation in suspensions of rod-like particles are those of Anselmet (1989). Results for an $a_r = 10$ rod-like particle system ($L = 1$ mm and $d = 0.1$ mm) are shown in Figure 5. These data are generally lower than ours. One possible explanation for this is that, despite the aspect ratio being smaller, the dimensions of the sedimentation vessels used in Anselmet's work were $1 \times 1 \times 4$ cm^3. Hence, the width of the vessel was only an order of magnitude larger than the fiber length, and so wall hindrance effects on the settling fibers may not be negligible.

Preliminary simulation results obtained by Mackaplow and Shaqfeh (1993) for rod-like particle suspensions having $a_r = 15.6$ are also shown in Figure 5. These simulations were performed with elongated spheroids in an isotropic orientation. These results tend towards our data at the larger volume fractions. At the lower volume fractions, there is a larger discrepancy, but this may result from larger effects due to interfacial spreading that result from variations in aspect ratio.

Conclusions

The sedimentation dynamics of rod-like particles are significantly different than those of spherical particle systems. These differences can be attributed in part to the differences in the relative viscosities and interparticle forces. An $a_r = 17.4$ rod-like particle suspension has considerably stronger hindered settling effect.

This work raises several points that warrant further study. While the strong effect of the aspect ratio on the hindered settling function has been established, there remains the need for quantitative determination of the hindered settling function over a wide range of aspect ratios. It is also necessary to establish the appropriateness of calculating U_o from an average over all orientations. Finally, the analysis of interfacial spreading needs to be undertaken, which yields information on hydrodynamic diffusivity and polydispersity for spherical particles.

Acknowledgments

This work has been supported by grants from the National Science Foundation, CBT-8718261 and CTS-9057660.

Notation

a_r = mean aspect ratio
d_e = diameter of a sphere that has the same volume as the fiber
g = acceleration due to gravity
h_o = height of the top of the suspension
$h(t)$ = height of a fiber at time t
K_1, K_2, K_3 = components of the principal translational resistance
S_b, S_b' = MRI signal intensity of the blank (suspending fluid only)
$S_{\infty b}$ = MRI signal intensity of the blank at $\tau \gg 5T_1$
S_s, S_s' = MRI signal intensity of the suspension
$S_{\infty s}$ = MRI signal intensity of the suspension at $\tau \gg 5T_1$
S_{os} = "T_2 corrected signal" of the suspension
S_1, S_2 = signal intensities 1 and 2 acquired by the FAVORITE pulse sequence to estimate spatially resolved T_1
t_e = echo time in Hahn spin-echo pulse sequence
U = mean particle settling velocity
U_1, U_2, U_3 = components of the terminal fall velocity of a single fiber
U_o = mean terminal settling velocity of a single fiber
V = volume occupied by a single fiber

Greek letters

μ = viscosity of suspending medium
μ_r = relative viscosity of suspension
τ = predelay time or delay time in the FAVORITE pulse sequence to measure T_1

Literature Cited

Anselmet, M.-C., "Contribution a L'Etude des Systemes Fluide-Particules: Suspensions de Cylindres, Lits Fluidises," Doctorate Diss., Univ. of Provence, France (1989).

Auzerais, F. M., R. Jackson, W. B. Russel, and W. F. Murphy, "The Transient Setting of Stable and Flocculated Dispersions," *J. Fluid Mech.*, **221**, 613 (1990).

Barnea, E., and J. Mizrahi, "A Generalized Approach to the Fluid Dynamics of Particulate Systems: I. General Correlation for Fluidization and Sedimentation in Solid Multiparticle Systems," *Chem. Eng. J.*, **5**, 171 (1973).

Becker, H. A., "Effects of Shape and Reynolds Number on Drag in the Motion of a Freely Oriented Body in an Infinite Fluid," *Can. J. Chem. Eng.*, **37**, 85 (1959).

Buscall, R., J. W. Goodwin, R. H. Ottewill, and Th. F. Tadros, "The Settling of Particles Through Newtonian and Non-Newtonian Media," *J. Colloid Interface Sci.*, **85**, 78 (1982).

Canet, D., J. Brondeau, and K. Elbayed, "Superfast T_1 Determination by Inversion-Recovery," *J. Mag. Res.*, **77**, 483 (1988).

Davis, R. H., and A. Acrivos, "Sedimentation of Noncolloidal Particles at Low Reynolds Numbers," *Ann. Rev. Fluid Mech.*, **17**, 91 (1985).

Davis, R. H., and M. A. Hassen, "Spreading of the Interface at the Top of a Slightly Polydisperse Sedimenting Suspension," *J. Fluid Mech.*, **196**, 107 (1988).

Fanni, J., D. Canet, K. Elbayed, and J. Hardy, "^{1}H and ^{23}Na NMR Relaxation Studies of the NaCl/β-Lactoglobulin System Equilibrated at Various Water Activities," *J. Food Sci.*, **54**, 909 (1989).

Flory, P. J., and G. Ronca, "Theory of Systems of Rodlike Particles," *Mol. Cryst. Liq. Cryst.*, **54**, 289 (1989).

Forgacs, O. L., and S. G. Mason, "Particle Motions in Sheared Suspensions IX. Spin and Deformation of Thread Like Particles," *J. Coll. Sci.*, **14**, 457 (1959).

Garside, J., and M. R. Al-Dibouni, "Velocity-voidage Relationship for Fluidization and Sedimentation in Solid-liquid Systems," *Ind. Eng. Chem. Process Des. Dev.*, **16**, 206 (1977).

Happel, J., and H. Brenner, "Low Reynolds Number Hydrodynamics: With Applications to Particulate Media," *Series in Mechanics of Fluids and Transport Processes*, M. Nijhoff, ed., Vol. 1, Kluwer Boston, Boston (1983).

Kauten, R. J., J. E. Maneval, and M. J. McCarthy, "Fast Determination of Spatially Localized Volume Fractions in Emulsions," *J. Food Sci.*, **56**, 799 (1991).

Lee, S., Y. Yang, C. Choi, and T. Lee, "Combined Effect of Sedimentation Velocity Fluctuation and Self-Sharpening on Interface Broadening," *Phys. Fluids A*, **4**, 2601 (1992).

Mackaplow, M., and E. S. G. Shaqfeh, "The Sedimentation of Fiber Suspensions at Dilute and Non-Dilute Concentrations," AIChE Meeting, St. Louis, MO (1993).

Maneval, J. E., M. J. McCarthy, and S. Whitaker, "Use of NMR as an Experimental Probe in Multiphase Systems: Determination of the Instrument Weight Function for Measurements of Liquid-Phase Volume Fractions," *Water Resour. Res.*, **26**, 2807 (1990).

Milliken, W. J., M. Gottlieb, A. L. Graham, L. A. Mondy, and R. L. Powell, "The Viscosity-Volume Fraction Relation for Suspensions of Randomly Oriented Rods by Falling-Ball Rheometry," *J. Fluid Mech.*, **202**, 217 (1989).

Morris, P. G., *Nuclear Magnetic Resonance Imaging in Medicine and Biology*, Oxford Univ. Press, Oxford, England (1986).

Morrison, T., "Experimental Investigation of the Mechanics of Suspensions of Elongated Particles Using Falling-Ball Rheometry," MS Thesis, Univ. of California, Davis (1989).

Powell, R. L., "Rheology of Suspensions of Rodlike Particles," *J. Stat. Phys.*, **62**, 1073 (1991).

Reinhart, W. H., A. Singh, and P. W. Straub, "Red Blood Cell Aggregation and Sedimentation: The Role of the Cell Shape," *Brit. J. of Hematology*, **73**, 551 (1989).

Richardson, J. F., and W. N. Zaki, "Sedimentation and Fluidization: I," *Trans. Inst. Chem. Eng.*, **32**, 35 (1954).

Russel, W. B., D. A. Saville, and W. R. Showalter, *Colloidal Dispersions*, Cambridge Univ. Press, Cambridge, England (1990).

Manuscript received Aug. 12, 1993, and revision received Mar. 21, 1994.